

# Harmonic analysis based modeling of tapping-mode AFM<sup>1</sup>

A. Sebastian<sup>1</sup>, M. V. Salapaka<sup>1</sup>, D. J. Chen and J. P. Cleveland<sup>2</sup>

<sup>1</sup> Dept. of Electrical Engineering,  
Iowa State University, Ames, Iowa 50011.

<sup>2</sup> Digital Instruments, Robin Hill Road  
Santa Barbara California 93117

## Abstract

In this paper we use harmonic balance and averaging techniques to analyze the tapping mode dynamics of the atomic force microscope. A model for the cantilever sample interaction is developed. Experimental results show that the analysis and the model predict the behavior of the tapping cantilever.

## 1 Introduction

The AFM (atomic force microscope) has revolutionized imaging in the last decade, having significant impact in diverse fields like physics, biology, and chemistry. The AFM has made it practical to achieve nanometer scale resolution in topography imaging.

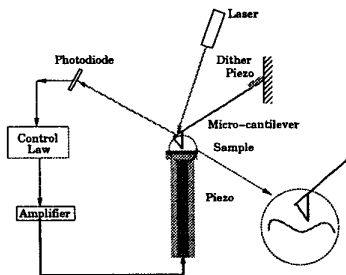


**Figure 1:** A schematic of an atomic force microscope. The sample to be imaged sits on a piezo tube which moves the sample in all the three directions. As the sample is moved beneath the micro-cantilever, the cantilever tip's deflection is registered by the resulting deflection of the laser incident on a position-sensitive photodiode.

The operation of a typical AFM is described in Figure 1 which consists of a micro-cantilever with a sharp tip, a sample positioning system, a detection system and a control system. One of the widely used modes of AFM imaging is the tapping-mode, where the cantilever is vibrated near its resonant frequency. The interaction between the tip and sample alters the ampli-

tude, phase, and resonant frequency of the cantilever oscillation which is monitored to infer properties of the sample. The dynamics of tapping-mode is considerably more involved than that of contact mode. Research has indicated that chaotic behavior is possible in certain parameter regimes [2, 7]. However, in most operating regimes the mode offers a robust way of imaging samples with high resolution.

Extensive research has been done on characterizing the tip-sample interaction and elaborate models have been developed in the scanning probe literature (e.g. [1]). In contrast to such methods, in this paper our focus will be to obtain as simple a model of the tip-sample interaction, as possible which predicts the essential features observed in experiments on the dynamics of tapping-mode. The dynamics of the amplitude and phase variables (which are important for imaging) are obtained by using the averaging method. It is shown that the fixed points of the averaged dynamics satisfy the harmonic balance equations. Time simulations of the dynamics assuming a piecewise linear sample-cantilever interaction are presented. Finally, experimental observations that have guided and that were prompted by the theoretical analysis are presented.

## 2 Tapping mode dynamics: modeling and analysis

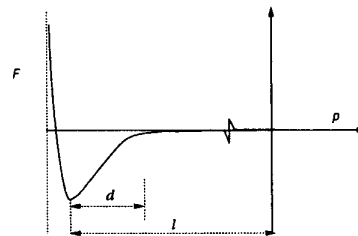


**Figure 2:** Sketch of a typical cantilever-sample force.

### 2.1 Modeling

In the tapping mode a dither piezo attached to the substrate that forms the support for the cantilever is forced sinusoidally.

The cantilever model dynamics are described by Figure 3. The dynamical equation of the tip of the can-

<sup>1</sup>Research supported by NSF grant ECS-9733802 and by ISU SPRIGS grant 7041747.

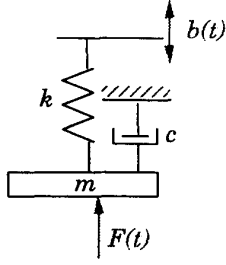


Figure 3: Model of the cantilever

tilever,  $p(t)$ ,

$$\ddot{p} + 2\xi\omega_0\dot{p} + \omega_0^2 p + h(p, \dot{p}) = g(t), \quad (1)$$

$\omega_0 = \sqrt{\frac{k}{m}}$ ,  $2\xi\omega_0 = \frac{c}{m}$  and  $g(t) = \frac{kb(t)}{m}$  and  $h$  is the force due to the sample per unit mass. A block diagram depicting the dynamics is given in Figure 4, where  $G$  is

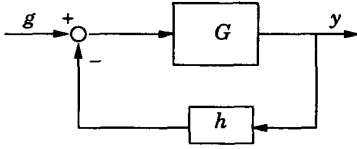


Figure 4: Block diagram

any linear model of the cantilever.

Experimental data has indicated that a force curve of the form shown in Figure 2 well characterizes the force on the cantilever due to the sample. It indicates long range attractive forces and short range strong repulsive forces.

## 2.2 Harmonic balance

We will assume that for the dynamics depicted by Figure 4 there exists a periodic orbit with the same period as that of  $g$  where  $g$  is sinusoidal (see [6]). We will denote such a periodic orbit by  $p_*(t)$ . Because the nonlinear force on the cantilever due to the sample is assumed to be time-invariant it follows that  $h(p_*, \dot{p}_*)$  is also periodic with period  $T$ . Thus  $p_*$ ,  $h(p_*, \dot{p}_*)$  and  $g(t)$  all admit expansions of the form  $p_*(t) = \sum_{k=-\infty}^{\infty} p_k e^{jk\omega t}$ ,  $h(p_*(t), \dot{p}_*(t)) = \sum_{k=-\infty}^{\infty} h_k e^{jk\omega t}$  and  $g(t) = \sum_{k=-\infty}^{\infty} g_k e^{jk\omega t}$ , where  $x_k = x_{kr} + jx_{ki}$  are the exponential Fourier coefficients of  $x$ . Note that on the periodic orbit Figure 4 can be viewed as illustrated in Figure 5. From the linearity of

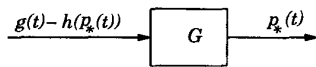


Figure 5: Harmonic balance.

the cantilever model  $G$  and the fact that  $p_*$  and  $h(p_*)$

are real signals it follows that

$$G(jk\omega)(g_k - h_k) = p_k \text{ for } k = 0, 1, 2, \dots \quad (2)$$

One of the intriguing features observed in experiments is that under normal operating conditions irrespective of the cantilever or the sample characteristics the periodic orbit is nearly sinusoidal. This can be explained as follows. The thermal noise response plots (both experimental and theoretical) of a typical cantilever indicate that  $|G(jk\omega)|$  (where  $G$  is a multimode model of the cantilever) is very small. This can be deduced from the study of thermal noise response in [5]. Thus one can assume that  $|G(jk\omega)| \approx 0$  for all  $k = 2, 3, \dots$ . It now follows immediately from Equation (2) that  $p_k = 0$  if  $|k| \geq 2$ . Thus one can write  $p_*(t) = a \cos(\omega t + \phi) + p_0$ , where  $a = 2|p_1|$  and  $p_1 = |p_1|e^{j\phi}$ . Thus the filtering effect of the cantilever transfer function results in a nearly sinusoidal orbit of the cantilever. We will assume that  $p_k$  is zero for  $|k| \geq 2$ . The harmonic balance equations reduce to

$$h_0 - g_0 + \omega_0^2 p_0 = 0 \quad (3)$$

$$h_{1r} - g_{1r} + \Omega \frac{a}{2} \cos \phi - 2\xi\omega\omega_0 \frac{a}{2} \sin \phi = 0 \quad (4)$$

$$h_{1i} - g_{1i} + 2\xi\omega\omega_0 \frac{a}{2} \cos \phi + \Omega \frac{a}{2} \sin \phi = 0. \quad (5)$$

where  $\Omega = \omega_0^2 - \omega^2$  and let  $\Delta := (\omega_0^2 - \omega^2)^2 + 4\xi\omega^2\omega_0^2$ . Note that  $p_{1r} = \frac{a}{2} \cos \phi$  and  $p_{1i} = \frac{a}{2} \sin \phi$ .

## 2.3 Connection to averaging

Consider a system of the form

$$\dot{x} = \epsilon f(x, t, \epsilon), \quad x \in R^n, \quad 0 \leq \epsilon \ll 1, \quad (6)$$

where  $f : R^n \times R \times R^+ \rightarrow R^n$  is periodic in  $t$  with period  $T$ . The associated autonomous averaged system is given by (see [4])

$$\dot{x}_a = \epsilon \frac{1}{T} \int_0^T f(x, t, 0) dt =: \epsilon f_a(x). \quad (7)$$

Note that the tapping mode dynamics is described by the equation  $\ddot{p} + \omega_0^2 p = \epsilon f(p, \dot{p}, t)$ , where  $f(p, \dot{p}, t) = \frac{g(t)}{\epsilon} - \frac{2\xi\omega_0\dot{p}}{\epsilon} - \frac{h(p, \dot{p})}{\epsilon}$ . We will assume that  $g$ ,  $2\xi\omega_0\dot{p}$  and  $h$  are quantities proportional to  $\epsilon$ . Define new variables  $u$  and  $v$  by

$$\begin{pmatrix} u \\ v \end{pmatrix} = \begin{pmatrix} \cos \omega t & -\frac{1}{\omega} \sin \omega t \\ -\sin \omega t & -\frac{1}{\omega} \cos \omega t \end{pmatrix} \begin{pmatrix} p - p_0 \\ \dot{p} \end{pmatrix}. \quad (8)$$

Let  $a = \sqrt{u^2 + v^2}$  and  $\phi := \arctan(\frac{v}{u})$ . Then we have  $p = a \cos(\omega t + \phi) + p_0$  and  $\dot{p} = -\omega a \sin(\omega t + \phi)$ . Assuming that the variables  $a$ ,  $\phi$  and  $\dot{p}$  are slowly varying, the averaged equations are given by

$$\dot{u}_a = \frac{1}{\omega} \left\{ -\Omega \frac{a_a}{2} \sin \phi_a - 2\xi\omega\omega_0 \frac{a_a}{2} \cos \phi_a + g_{1i} - h_{1i} \right\} \quad (9)$$

$$\dot{v}_a = \frac{1}{\omega} \left\{ \Omega \frac{a_a}{2} \cos \phi_a - 2\xi\omega\omega_0 \frac{a_a}{2} \sin \phi_a + h_{1r} - g_{1r} \right\}. \quad (10)$$

Relating the harmonic balance equations given by (4) and (5) to equations (9) and (10) we see that the harmonic balance equations indeed yield the fixed points of the averaged dynamics. Thus by solving the harmonic balance equations for the variables  $a$ ,  $\phi$  and  $p_0$  and finding out the stability type of the related fixed point we can determine the amplitude, phase and the stability of the periodic orbit.

If we further assume that the cantilever-sample interaction is conservative and that the cantilever-sample force is given by the derivative of a potential  $V(p)$  (that is  $h = \frac{\partial V}{\partial p}$ ) then it follows that  $h_{1r} \sin \phi - h_{1i} \cos \phi = 0$ . Similarly it can be shown that  $h_{1r} \cos \phi + h_{1i} \sin \phi = \frac{1}{2\pi} \int_0^{2\pi} \frac{\partial V}{\partial p}(p_0 + a \cos \psi) \cos \psi d\psi =: \bar{g}(a, p_0)$ . Note that  $\bar{g}$  is independent of the variable  $\phi$ . With these relations we have

$$\dot{a}_a = \frac{1}{\omega} \left\{ -\frac{a_a}{2} 2\xi\omega_0\omega - \frac{\gamma}{2} \sin \phi_a \right\} \quad (11)$$

$$\dot{\phi}_a = \frac{1}{\omega a_a} \left\{ \frac{a_a}{2} \Omega + \bar{g}(a_a, p_0) - \frac{\gamma}{2} \cos \phi_a \right\}. \quad (12)$$

Solving for the fixed points we see that

$$a_a = \frac{\gamma}{\sqrt{4\xi^2\omega_0^2\omega^2 + (\Omega + \frac{2\bar{g}(a_a, p_0)}{a_a})^2}}, \quad \tan \phi = \frac{-2\xi\omega_0\omega}{\Omega + \frac{2\bar{g}(a_a, p_0)}{a_a}}. \quad (13)$$

Setting the right hand side of Equation (11) we obtain

$$a_a = \frac{\gamma}{2\xi\omega_0\omega} \sin \phi_a \quad (14)$$

which predicts a linear relationship between  $\sin \phi$  and the amplitude  $a$  (see [3] also).

#### 2.4 Piecewise linear model of the sample interaction

In this part of the paper we will assume a piecewise linear cantilever-sample force curve (see Figure 6). Specifically we assume that

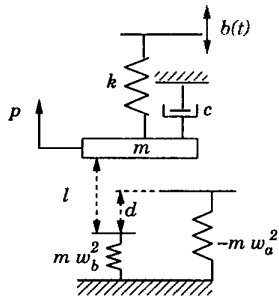


**Figure 6:** Model with the piecewise linear cantilever sample force interaction.

$$h(p) = 0 \text{ if } p \geq -l + d \quad (15)$$

$$= -\omega_a^2(p + l - d) \text{ if } -l \leq p < -l + d \quad (16)$$

$$= \omega_b^2(p + l) - \omega_a^2(p + l - d) \text{ if } p < -l. \quad (17)$$

The coefficients  $h_0$  and  $h_1$  are given in Equation (18) where  $s_1 = \frac{-l + d - p_0}{a}$  and  $s_2 = \frac{-l - p_0}{a}$ . Using

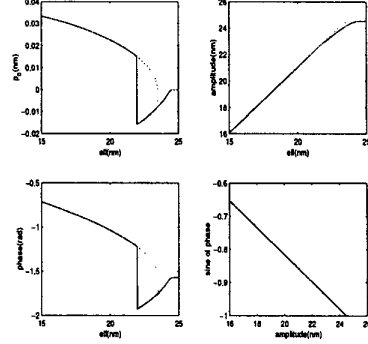


**Figure 7:** The time simulation plots resulted in solid curve (which coincided with the harmonic solutions obtained by harmonic balance) when the sample was slowly moved towards the cantilever and the dotted curve when the sample was moved away from the cantilever. The bistable behavior is clear from the hysteric behavior. The plot of the sine of the phase versus the amplitude shows the linear relationship between the two parameters.

Simulink the response of the system shown in Figure 6 was obtained for  $f_0 = 299.95 \text{ KHz}$ ,  $\omega_0 = \omega = 2\pi f_0$ ,  $\omega_a = 0.5\omega_0$ ,  $\omega_b = 10\omega_0$ ,  $d = 1 \text{ nm}$  and  $Q = \frac{1}{2\xi} = 275$ . The forcing magnitude was such that the steady state amplitude of the cantilever tip oscillation in the absence of the sample was  $24.5 \text{ nm}$  with  $k \approx 29 \text{ N/m}$ . In the simulation the variable  $l$  was slowly decreased from  $30 \text{ nm}$  to  $15 \text{ nm}$  (the approach), and then increased slowly from  $15 \text{ nm}$  to  $30 \text{ nm}$  (the retract). As is evident from Figure 7 when the sample is approaching the cantilever, the phase and amplitude (shown by the solid line) show a discontinuity at a lesser value of  $l$  than when the sample is retracting from the cantilever (shown by the dotted line). It is also evident that the sine of the phase varies linearly with respect to the amplitude (no signature of hysteric behavior is present in this plot). This was predicted by Equation (14). It was also verified that the amplitude and the phase variables satisfied the harmonic balance Equations (3), (4) and (5). Note that in deriving the parameters  $h_0$  and  $h_1$  in the harmonic balance equations, it was assumed that the cantilever motion was purely sinusoidal. In the time simulation no such assumptions are made where the amplitude and the phase of the first harmonic of  $p$  are obtained. That the amplitude and the phase of the first harmonic in the time simulations agree with the amplitude and phase of harmonic balance equations indicates that the assumption on ignoring the higher harmonics of  $p$  in obtaining the harmonic balance equations is justified.

$$\begin{aligned}
h_0 &= 0 \text{ if } p_0 - a \geq -\ell + d \\
&= \frac{a\omega_a^2}{\pi}(\sqrt{1-s_1^2} - |s_1| \cos^{-1}(|s_1|)) \text{ if } -\ell \leq p_0 - a < -\ell + d \\
&= \frac{a\omega_a^2}{\pi}(\sqrt{1-s_1^2} - |s_1| \cos^{-1}(|s_1|)) - \frac{a\omega_b^2}{\pi}(\sqrt{1-s_2^2} - |s_2| \cos^{-1}(|s_2|)) \text{ if } p_0 - a < -\ell \\
\bar{g}(a, p_0) &= 0 \text{ if } p \geq -\ell + d \\
&= \frac{a\omega_a^2}{2\pi^2}(|s_1|\sqrt{1-s_1^2} - \cos^{-1}(|s_1|)) \text{ if } -\ell \leq p_0 - a < -\ell + d \\
&= \frac{a}{2} \frac{\omega_a^2}{\pi^2}(|s_1|\sqrt{1-s_1^2} - \cos^{-1}(|s_1|)) - \frac{a}{2} \frac{\omega_b^2}{\pi^2}(|s_2|\sqrt{1-s_2^2} - \cos^{-1}(|s_2|)) \text{ if } p_0 - a < -\ell \\
h_{1r} &= \bar{g}(a, p_0) \cos \phi \\
h_{1i} &= \bar{g}(a, p_0) \sin \phi
\end{aligned} \tag{18}$$

### 3 Experimental methods

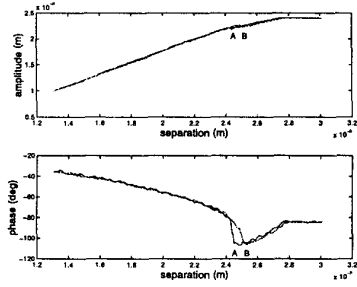


**Figure 8:** Experimental data when the sample, positioned by the piezo tube, approaches and retracts from the cantilever. The amplitude and phase of the cantilever motion while approaching and retracting are the same except for the part between points A and B. This bistable behavior is characteristic of the Tapping mode operation.

An atomic force microscope (Multi-Mode, Digital Instruments, Santa Barbara, CA) was operated in the Tapping Mode. A silicon cantilever of length 225 microns was used. The model parameters were evaluated by analyzing the cantilever response to thermal noise in similar ways to those suggested in [5]. The cantilever parameters were found to be  $\omega_0 = 2\pi \times 73881$  rad/sec,  $\xi = 0.0038$  and  $k_0 = 4\text{N/m}$ . A sinusoidal voltage with its frequency equal to the resonant frequency  $\omega_0$  of the cantilever was applied to the dither piezo (see Figure 1). The motion of the cantilever tip at various values of the

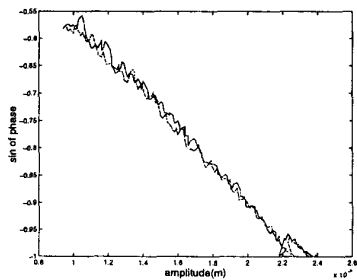


**Figure 9:** Sine of the phase plotted against amplitude.

piezo extension was recorded using an HP 89410 Vector Signal Analyzer or a Stanford Research SR530 2-phase

lock-in amplifier. A feature of the experimental data is illustrated by Figure 8. It is seen that as the sample is moved (relatively slowly) towards the cantilever (moved upwards in Figure 1) the oscillation amplitude decreases linearly with decreasing average cantilever-tip sample separation. The decay is monotonic for most of the traversal except for a discontinuity at a value A. At the same point there is a jump in the phase also (the phase is the amount by which the sinusoidal deflection of the cantilever tip lags behind the forcing). On retracting the sample away from the cantilever (the sample is moved downwards in Figure 1) the same behavior is observed except that the discontinuity appears at a larger value B (for experimental details see [3]). The hysteresis effect is indicative of the bistable behavior in the system typical of the tapping mode dynamics. Note that this bistable behavior was also predicted by the model with a piecewise linear cantilever sample force interaction (compare Figure 7 with Figure 8). The sine of the phase versus amplitude plot is shown in Figure 9. For most of the sample traversal the plot is linear. The linear relationship is predicted by Equation (14) assuming a conservative sample cantilever interaction. The deviation from the linear relation and the fact that the slope is slightly smaller than predicted by (14) are attributed to non-conservative terms in the tip-sample interaction. The mismatch of the experimental data in satisfying the harmonic balance equation can be used to infer sample properties. Also, the parameters  $\ell, d, \omega_a$  and  $\omega_b$  in Figure 6 can be identified using experimental data.

### 4 Estimation

A linear relationship can be established between the coefficients  $h_0$  and  $h_1$  and the spring constants  $\omega_a^2$  and  $\omega_b^2$  using Equations (18). This allows us to estimate the spring constants given amplitude, phase and  $p_0$  for different values of  $l$ . However  $p_0$  is very difficult to measure due to its relatively small magnitude. Thus it becomes essential to ascertain if various parameters in the model can be estimated by letting  $p_0$  to be zero. The simulation data was used to study the impact of  $p_0$  on the coefficients  $h_0$  and  $h_1$ . It was found that  $p_0$  affects  $\omega_b$ . However its effect on  $\omega_a$  is negligible. Similar plots were obtained for  $h_0$  and  $h_{1r}$ . Hence a reasonable estimate of  $\omega_a$  can be obtained. But the estimation of

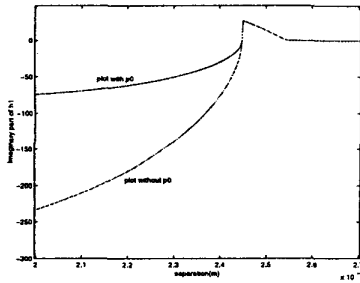


**Figure 10:** The imaginary part of  $h_1$  is plotted against  $l$  for the simulation data for two cases. In one case  $p_0$  is assumed to be known whereas in the second case  $p_0$  is set to zero. It can be seen that the plots almost overlap in the attractive region.

$\omega_b$  is difficult without knowing  $p_0$ . An estimation of  $\omega_a$  was made using the simulation data for the attractive region without using  $p_0$  to verify the observation. Estimates were very close to the  $\omega_a$  value used for the simulation. This idea was extended to the experimental data. It was assumed that the amplitude of vibration is approximately equal to the distance of separation in the repulsive region. This assumption is reasonable because the repulsive forces are strong enough and do not allow any significant penetration into the sample. The strong dependence of the coefficients of  $h$  on  $p_0$  (which is very small in magnitude) in the repulsive region is an added justification.  $l$  was fixed by the above argument. When amplitude is plotted against  $l$ , there is a distinct change in slope between the attractive and repulsive regions. This is used to fix  $d$ . The real and imaginary parts of  $h_1$  were evaluated using the part of the experimental data corresponding to the attractive region alone. The harmonic balance equations were used for this purpose.  $h_0$  couldn't be evaluated due to the explicit dependence of  $h_0$  on  $p_0$ . A least square estimate of  $\omega_a$  was obtained using the  $h_1$  values.  $\omega_a$  was estimated to be  $1.4061e5$  which is approximately  $0.3029 * \omega_0$ . The estimated  $\omega_a$  value was used to simulate the model. The amplitude and phase plots thus obtained were compared (in the attractive region) with the plots obtained using experimental data. Using the estimated value of  $\omega_a$  we can evaluate  $h_0$  using Equation (18). Since in the attractive region  $h_0$  values do not change much by letting  $p_0$  to zero, the harmonic balance equations combined with Equation (18) were used to arrive at an estimate for  $p_0$ .

## 5 Conclusions

In this paper it is shown that many of the experimentally observed features in tapping mode atomic force microscopy can be explained by the harmonic balance technique. It is also shown that the same conclusions can be reached via averaging techniques. Also both predicted behavior which was later confirmed by experimental data. A piecewise linear model was con-

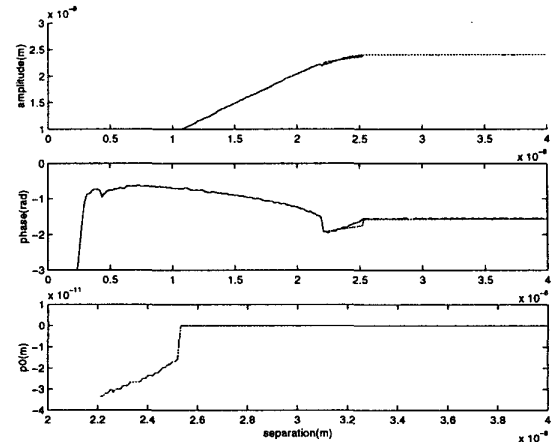


**Figure 11:** Using the estimated  $\omega_a$ , plots of amplitude and phase are obtained for the attractive region and are compared with plots obtained using experimental data. Also shown is a plot of the estimated  $p_0$ .

structed for the cantilever-sample interaction which captured the essential characteristics of the experimentally observed behavior of the tapping cantilever. The harmonic balance provides a computationally efficient method for evaluating the phase and the amplitude for such a model.

## References

- [1] B. Anczykowski, D. Kruger, K. L. Babcock, and H. Fuchs. Basic properties of dynamic force spectroscopy with scanning force microscope in experiment and simulation. *Ultramicroscopy*, 66/3-4, 1997.
- [2] M. Ashhab, M. V. Salapaka, M. Dahleh, and I. Mezic. Dynamical analysis and control of micro-cantilevers. *Accepted: Automatica*, 1998.
- [3] J. P. Cleveland, B. Anczykowski, A. E. Schmid, and V. B. Elings. Energy dissipation in tapping-mode atomic force microscopy. *Applied Physics Letters*, 72, no. 20:pp. 2613-2615, 1998.
- [4] J. Guckenheimer and P. Holmes. *Nonlinear oscillations, dynamical systems, and bifurcations of vector fields*. Springer Verlag, New York, 1983.
- [5] M. V. Salapaka, H. S. Bergh, J. Lai, A. Majumdar, and E. McFarland. Multimode noise analysis of cantilevers for scanning probe microscopy. *Journal of Applied Physics*, 81(6):2480-2487, 1997.
- [6] M. V. Salapaka, D. J. Chen, and J. P. Cleveland. Stability and sensitivity analysis of periodic orbits in tapping mode atomic force microscopy. In *Proceedings of the IEEE Conference on Decision and Control*. Tampa, Florida, December 1998.
- [7] S. M. Salapaka, M. V. Salapaka, M. Dahleh, and I. Mezic. Complex dynamics in repeated impact oscillators. In *Proceedings of the IEEE Conference on Decision and Control*. Tampa, Florida, 1998.